ACS APPLIED MATERIALS & INTERFACES

Research Article

www.acsami.org

Etch-Free Patterning of Poly(3,4-ethylenedioxythiophene)−Poly(styrenesulfonate) for Optoelectronics

Steven A. Rutledge and Amr S. Helmy*

Edward S. Rogers Sr. Department of Electrical and Computer Engineering, University of Toronto, Toronto M5S 3G4, Canada

Supporting Information

ABSTRACT: Spatial control of the conductivity of poly(3,4-ethylenedioxythiophene)−poly(styrenesulfonate) (PEDOT:PSS) is demonstrated through the use of ultraviolet (UV) exposure. With appropriate UV exposure, electrical characterization shows that the in-plane sheet resistance of PEDOT:PSS films is increased by 4 orders of magnitude compared to unexposed regions. Characterization of the films using Raman spectroscopy identifies a significant reduction of the inter-ring stretching modes between PEDOT monomers and a morphological shift from the quinoid to benzoid form of PEDOT. Additional analysis using Fourier transform infrared spectroscopy indicates a reduction in film doping and a decrease in C═C vibrational modes that are associated with PEDOT oligomer length. Height and phase images of these films obtained from atomic force microscopy exhibit a loss of phase segregation in the film between the PEDOT grains and PSS regions. Spectroscopic ellipsometry highlights an increase in both the real and imaginary components of the index upon UV exposure. This broad range of analysis consistently suggests that the increased resistivity can be attributed to a significant reduction in material doping caused by scission-driven decomposition of the conductive PEDOT chains. When flood exposure is combined with the use of an appropriate UV blocking mask, patterning in the conductivity of PEDOT:PSS films can be realized. In contrast to other patterning approaches, no resist development or etching is required for the electrical isolation of certain regions. To demonstrate the efficacy of this process, an organic light emitting diode was fabricated with UV-patterned PEDOT:PSS as a hole transport layer. The regions of unexposed PEDOT:PSS produced electroluminescence, whereas those exposed to UV remained unlit, enabling the realization of pixelated illumination with no removal of material.

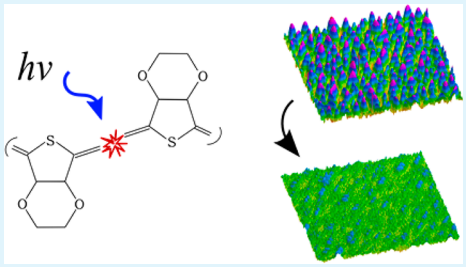

KEYWORDS: *PEDOT:PSS, organic patterning, optoelectronics, conducting polymer, OLED*

INTRODUCTION

Polymer and organic materials have developed to become a highly desirable platform for use in electronic and optoelectronic devices. In contrast to traditional all-inorganic electronic devices, organic materials offer a number of attractive and exciting advantages, including mechanical flexibility, being relatively lightweight, and having a low material cost coupled with low-cost fabrication methods.[1] Organic materials, however, suffer from several inherent drawbacks, including reliability, lower carrier mobility, and environmental degradation. One of the promising alternatives within the spectrum of conducting organic polymers is poly(3,4-ethylenedioxythiophene)−poly(styrenesulfonate) (PEDOT:PSS), which has been investigated extensively for use in electronic and optoelectronic applications. PEDOT:PSS is known to organize into two distinct morphologies, benzoid and quinoid, upon deposition, which are depicted in Figure 1a and b, respectively. The quinoid form of PEDOT is preferential for creating a linear or expanded-coil structure, which subsequently results in stronger interactions between subsequent polymer chains and enhanced conductivity.[2]

PEDOT:PSS has been studied for use in organic light emitting diodes (OLEDs), photovoltaics, thin film transistors, and other applications due to its favorable conductivity, optical transparency, and solubility in water.[3] PEDOT is a conductive polymer that is copolymerized with insulating PSS to generate a water-soluble colloidal solution. When spin-cast into a thin film, PEDOT:PSS has been found to maintain phase segregation between the PEDOT and PSS components, where a lamellar structure of conductive PEDOT regions is created and surrounded by thin, insulating PSS shells.[4] Although PEDOT:PSS offers relatively high conductivity when compared to other polymer or organic materials, it is still significantly less conductive than its inorganic transparent counterparts (e.g., indium tin oxide has a material conductivity of ∼10,000 S/cm, whereas even the most conductive PEDOT:PSS films are often less than that by more than an order of magnitude).[5] Another challenge with PEDOT:PSS is the limited selection of suitable techniques available for its patterning. Patterning of PEDOT:PSS has been addressed primarily using techniques that serve to selectively remove or deposit the polymer. A variety of different approaches, including soft lithography, contact imprinting, laser ablation, and shadow masking, have been developed.[6−8] Each of these approaches poses certain

Received: August 28, 2014
Accepted: January 29, 2015
Published: January 29, 2015

DOI: 10.1021/am507981d
ACS Appl. Mater. Interfaces 2015, 7, 3940−3948

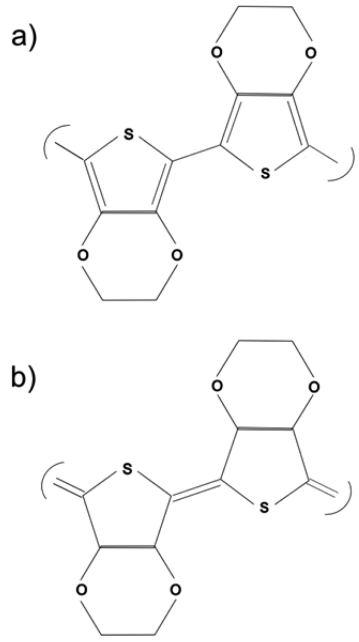

Figure 1. (a) Benzoid and (b) quinoid conformations of PEDOT.

process limitations that may not be suitable for all applications. The most common techniques of polymer patterning are inkjet printing and vacuum deposition of an inorganic layer through a shadow mask for device definition.[9] Both have limitations with respect to feature size and compatibility with other active and structural layers in a device. Direct ultraviolet (UV) exposure has been implemented with some success for photopatterning organic semiconductors whereby exposure changes the solubility of the material, allowing for facile material removal.[10,11]

UV exposure or UV-ozone treatments have previously been investigated as a means to alter the PEDOT:PSS work function for precise engineering of carrier transport in optoelectronic devices through energy level matching. Previous work indicates that the use of UV irradiation on a PEDOT:PSS film results in an increase in the polymer work function. However, there are additional, and occasionally contradicting, reports in the literature on the effects of UV exposure with respect to conductivity, solubility, and surface roughness.[12−17] Although PEDOT:PSS is transparent at visible wavelengths of electromagnetic radiation, it has been shown to suffer from significantly reduced conductivity upon exposure to high energy gamma and X-ray radiation due to scission, creating free radicals. This process serves to disrupt conductivity pathways through the polymer strands.[18] Previous reports have deduced that the conductivity of PEDOT:PSS is susceptible to degradation upon exposure to UV light, especially at wavelengths below 320 nm.[19] Although this effect has traditionally been perceived as a detriment to various applications, it could also be engineered to introduce spatial patterning in film conductivity.

This work demonstrates a viable technology to provide patterned devices without the need for etching the polymer layers. In conjunction with this demonstration, spectroscopic analysis explaining the basis for how this technology functions is also included. This spectroscopic analysis presents an in-depth investigation of the process and mechanisms associated with spatially defining conductive patterns in PEDOT:PSS films without the need for layer etching. The uniqueness of this technique lies in the fact that not only is a single exposure step required in the fabrication of an OLED device but also that the effects of the exposure are not limited to conductivity reduction. Other effects, such as spatial modulation of the film height as well as the refractive index of the PEDOT:PSS film, are also modified.

EXPERIMENTAL SECTION

For thin film deposition, PEDOT:PSS under the brand name Clevios F HC was filtered through a 0.22 μm Micropore filter and spin-cast onto three different substrates. These substrates included Corning glass 2947, indium tin oxide (ITO) on a boroaluminosilicate glass with a sheet resistance of 4−10 Ω/sq purchased from Delta Technologies, and a Si wafer. The spin parameters were such that the films on glass and ITO substrates resulted in an initial thickness of ∼100 nm, whereas the films on silicon were deposited with an initial thickness of ∼200 nm to obtain a higher signal-to-noise ratio for optical characterization. Following the deposition, a 10 min bake was performed at 150 °C to remove any residual water from the polymer films. The PEDOT:PSS films were then exposed to UV flood radiation in a Spectroline XL-1500 UV Cross-linker at three separate doses of 24.9, 48.3, and 71.6 J/cm^2. Electrical characterization of the sheet resistance was analyzed using four point probe model 101C from Four Dimensions. To characterize electrical conduction through the film normal to the substrate, Al contacts were thermally evaporated through a shadow mask onto the PEDOT:PSS films on ITO, and the $I-V$ characteristics were obtained using an HP4155 semiconductor parametric analyzer. Atomic force microscopy (AFM) images were generated using a Dimension 3100 AFM from Digital Instruments. Raman spectra of the films spun on Si were obtained using an HR800 Raman spectrometer manufactured by Horiba Jobin Yvon. Fourier transform infrared spectroscopy (FTIR) was performed on a Bruker Tensor II between 4000 and 800 cm^{-1} with a resolution of 2 cm^{-1}. Ellipsometric characterization was performed using a UVISEL ellipsometer manufactured by Horiba Jobin Yvon across the wavelength range from 0.6 to 5.0 eV with steps of 0.1 eV.

Patterned OLED devices were fabricated for demonstration by first depositing the PEDOT:PSS film on ITO as outlined above and subsequently exposing the PEDOT:PSS film to UV radiation through a UV blocking shadow mask, spin-casting poly[2-methoxy-5-(2-ethylhexyloxy)-1,4-(*p*-phenylenevinylene] (MEH:PPV) to a thickness of 90 nm and then depositing Al on top of the MEH:PPV to act as a cathode.

RESULTS AND DISCUSSION

PEDOT:PSS usually spin-casts into films with a lamellar structure in which there is distinct phase separation between the PEDOT and PSS polymers. This leads to films with an anisotropic morphology in which the conductive PEDOT grains are formed in stacked regions separated by thin insulating PSS.[4] This enables different transport mechanisms of current conduction with three-dimensional variable range hopping dominating in the lateral direction relative to the substrate and nearest neighbor hopping in the normal direction. Subsequently, the conductivity orthogonal to the substrate is lower by up to 3 orders of magnitude relative to the in-plane or lateral direction.[4] It is thus necessary to analyze both orientations of current transport with respect to any changes upon UV exposure.

Figure 2 displays the changes in the measured sheet resistance values with respect to exposure. These values are obtained by averaging ten separate measurements across the samples. The film thicknesses from AFM analysis are shown in Table 1. As the exposure energy increases, the sheet resistance is observed to increase progressively by over 4 orders of

DOI: 10.1021/am507981d
ACS Appl. Mater. Interfaces 2015, 7, 3940−3948

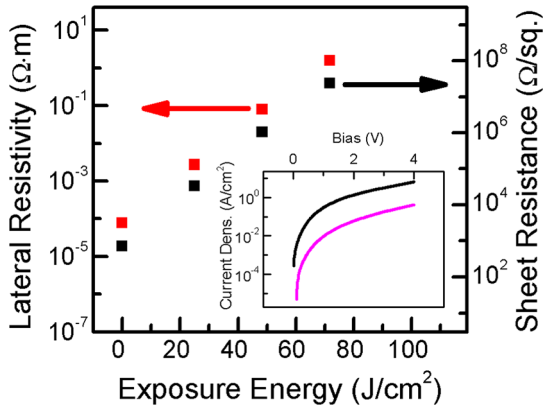

Figure 2. Changes in lateral (in-plane) material resistivity (red squares) and measured sheet resistance (black circles) as a function of the UV exposure energy. The colored arrows direct the respective colored data to the appropriate axis. (inset) *I*−*V* curves obtained for ITO/PEDOT:PSS/Al planar diode devices. The black solid line uses unexposed PEDOT:PSS, whereas the magenta line uses PEDOT:PSS that is exposed to 71.6 J/cm^2 of energy.

Table 1. PEDOT:PSS Film Thicknesses as a Function of UV Exposure

UV exposure (J/cm^2)	thickness (nm)
0	108
24.9	80
48.3	74
71.6	66

magnitude and at the same time, the measured thickness of the films decreases. As sheet resistance is dependent on the thickness of the thin film, multiplying the sheet resistance value by the measured thickness gives a value for material resistivity, which is displayed on a separate axis in Figure 2.

In contrast to the increased sheet resistance of 4 orders of magnitude, vertical transport conduction decreases by just over a factor of 10 as shown by the comparison of *I*−*V* curves in the inset of Figure 2. This anisotropy will have implications when utilizing this technique in optoelectronic devices; however, it may be engineered into the design of the devices to provide useful functionality.

Raman spectroscopy was performed on samples having undergone UV exposure. Figure 3 shows the complete spectrum of the PEDOT:PSS films grown. A number of Raman modes can be identified and attributed to both the PEDOT film and the underlying substrate correlating to previously identified Raman modes.[20] A regime of particular interest is between 1200 and 1600 cm^{-1}, where a number of Raman modes associated with the morphological strcuture of PEDOT:PSS films have previously been observed. The Raman spectra obtained from samples exposed to different levels of UV irradiation are shown in the inset of Figure 3 with the unexposed film being the bottom plot (black line). After the baseline was removed and the data was fitted with Gaussian−Lorentzian peaks, two specific modes were observed to clearly change with increased exposure and are highlighted with asterisks in the Figure 3 inset.

The mode at ∼1250 cm^{-1} is identified as a C_α−C_α inter-ring stretch, and the broader peak at ∼1450 cm^{-1} is a convolution of two separate symmetric C_α−C_β (−O) stretching modes dependent on a benzoid or quinoid PEDOT structure.[21,22]

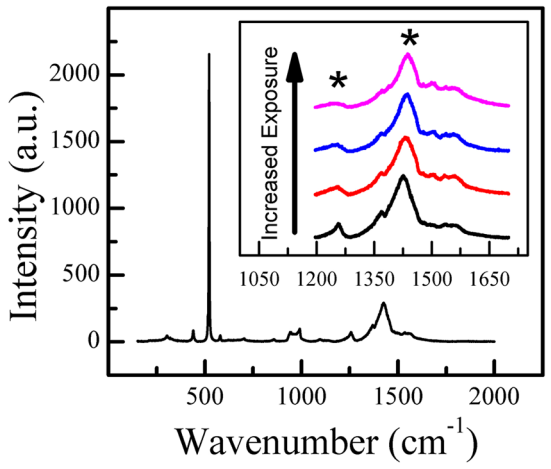

Figure 3. Raman spectra of unexposed PEDOT:PSS films on Si. (inset) Enhancement of the 1000−1700 cm^{-1} region to better visualize changes with respect to increasing UV exposure. The black, red, blue, and magenta curves were exposed to 0, 24.9, 48.3, and 71.6 J/cm^2 of UV radiation, respectively. Two Raman modes of particular interest are identified with asterisks: a C_α−C_α inter-ring stretch at ∼1250 cm^{-1} and a symmetric C_α−C_β (−O) stretching mode at ∼1450 cm^{-1}.

With the focus on the inter-ring stretching mode at 1250 cm^{-1} first, Table 2 lists the amplitudes of the inter-ring stretch

Table 2. Amplitude and Location of the C_α−C_α Inter-Ring Stretching Mode

UV exposure energy (J/cm^2)	normalized amplitude	central wavenumber (cm^{-1})
0	0.207	1255
24.9	0.126	1252
48.3	0.099	1251
71.6	0.081	1250

mode normalized to the magnitude of the 1450 cm^{-1} convolution peak, as well as the central wavenumbers of the associated peaks, at varying levels of UV exposure.[20]

Two distinct inter-ring stretching mode changes are identified as a result of increased UV exposure: the amplitude of the peak decreasing sharply to below 40% of its original value and a moderate blue shift in the mode. Although UV degradation of PEDOT:PSS conductivity has been attributed primarily to an enhanced oxidation rate, Raman results indicate an additional mechanism of degradation. Reduction of the normalized amplitude indicates a significant decrease in the overall contribution of inter-ring bonds between EDOT monomers. This is indicative of a scission process that occurs in the PEDOT chain and has previously been observed in PEDOT:PSS when exposed to higher energy radiation.[18] A scission process and subsequent PEDOT chain length reduction correlate with the significant increase in material resistivity as observed by electrical characterization. As bonds along the conductive polymer backbone chains are broken, the relatively efficient conduction mechanism is interrupted due to an increase in chain defects that result in a different transport process dominating the conduction; namely, the additional hopping events required between conductive PEDOT regions. It is, however, important to note that all other Raman peaks associated with the PEDOT polymer are maintained,

DOI: 10.1021/am507981d
ACS Appl. Mater. Interfaces 2015, 7, 3940−3948

confirming that the material is still intact and not significantly carbonized.[20]

The second peak of interest is convolution of $C_\alpha-C_\beta$ (−O) stretching modes in the ∼1450 cm^{-1} regime. As identified above, this peak is a combination of peaks at ∼1440 and ∼1465 cm^{-1} attributed to the quinoid and benzoid conformation structures, respectively.[20] Both forms of PEDOT are generally found in spin-cast thin films and can be used as indicators for determining the relative morphology of PEDOT samples. The benzoid form is often correlated with a coil conformation of the polymer chain, whereas the quinoid form preferentially forms a linear conformation. Of the two, the quinoid form provides higher sheet conductivity of the PEDOT:PSS thin film and is therefore the preferred form for charge conduction.[2] Figure 4

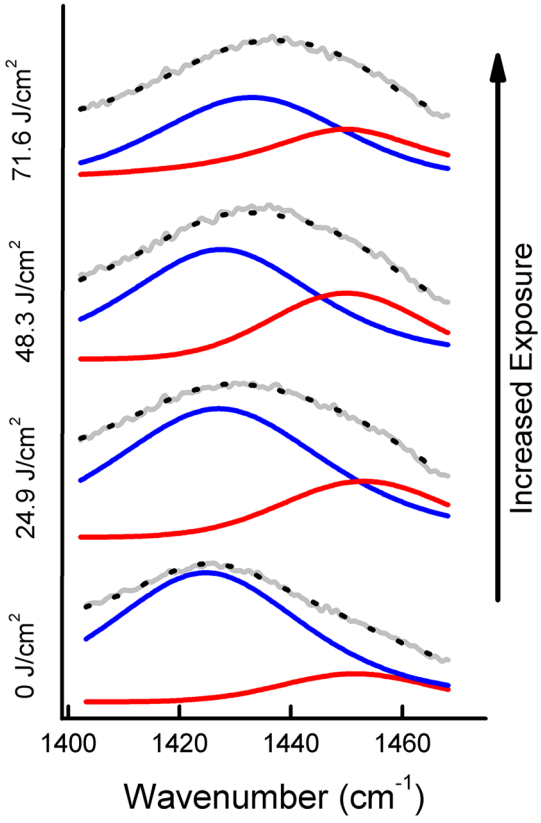

Figure 4. Detailed fitting of the $C_\alpha-C_\beta$ (−O) Raman mode composed of individual benzoid and quinoid peaks. The baseline corrected raw spectrum is shown in gray. The black dotted line displays the contributions of both modes to the measured data. The quinoid contribution (blue) is centered around 1430 cm^{-1}, and the benzoid contribution (red) is centered around 1450 cm^{-1}.

displays the measured spectra between 1400 and 1470 cm^{-1} (gray line), along with the individual quinoid (blue line) and benzoid (red line) peak fits as well as the complete fit for all of the samples characterized (black dashed line). Analysis of the fitted quinoid and benzoid peaks demonstrates that with increased UV exposure the chain morphology shifts from its initial state of being primarily quinoid to a much more balanced combination of the two modes. Table 3 displays the relative amplitude ratio of the quinoid to benzoid peaks along with their center wavenumbers.

In a trend similar to the inter-ring amplitude ratio, it is observed that with increasing UV exposure, the ratio of the quinoid to benzoid form of PEDOT progressively decreases.

Table 3. Analysis of the $C_\alpha-C_\beta$ (−O) Stretching Mode

UV exposure energy (J/cm^2)	quinoid/benzoid amplitude ratio	benzoid peak center (cm^{-1})	quinoid peak center (cm^{-1})
0	4.67	1451	1421
24.9	1.94	1451	1426
48.3	1.66	1450	1428
71.6	1.62	1450	1433

Additionally, whereas the benzoid peak is relatively stable, the Raman mode corresponding to the quinoid form progressively red shifts from 1421 cm^{-1} in the unexposed sample to 1433 cm^{-1} at 71.6 J/cm^2. The relative increase of the benzoid form of PEDOT with UV exposure correlates with an increase in sheet resistance measurements. Scission of the polymer chains may additionally introduce dangling bond sites that are prone to oxidative reactions and subsequent reorganization into a benzoid form of PEDOT.

When the overall Raman results are assessed, the observed resistivity increase may be attributed to both a scission process that reduces the polymer chain length and a morphological shift from a quinoid-dominant PEDOT film to one with significant benzoid composition. This morphological shift may be an independent effect of UV irradiation or it may be a consequence of the aforementioned polymer scission.

In combination with the Raman studies, FTIR was performed to further investigate changes to PEDOT:PSS film morphology. Raw spectra for the four PEDOT:PSS films are shown in Figure 5. The spectra have not been adjusted,

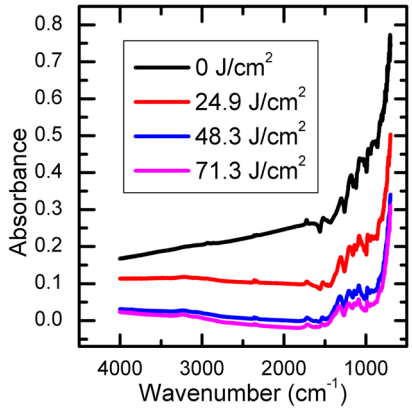

Figure 5. Raw spectra collected by FTIR across the range of 800–4000 cm^{-1}. The unexposed film and films irradiated with 24.9, 48.3, and 71.6 J/cm^2 are shown with black, red, blue, and magenta lines, respectively.

indicating that the resulting offset is due to changes in infrared (IR) light absorption. Although quantifying the magnitude of the IR absorption effect on conductivity is difficult, the previously identified 4 orders of magnitude reduction in conductivity is also evident in the spectral region between 2000 and 4000 cm^{-1}. In highly conductive PEDOT, the large concentration of free carriers in the film contributes to a high level of IR absorption above 2000 cm^{-1}.[2,3] There is a clear decline of IR absorption with UV exposure due to a corresponding decrease in the concentration of free charge carriers in the PEDOT film. Although this does not explicitly indicate a scission event, it aligns with the previous observation of a reduction in material conductivity. Vibrational modes evident in the films occur primarily within the range of 800–

DOI: 10.1021/am507981d
ACS Appl. Mater. Interfaces 2015, 7, 3940−3948

1700 cm^{-1}, which is in good agreement with theoretical and experimental expectations.[21,23−25]

After a baseline fitting routine was performed, the modes of interest became significantly clearer, and individual absorption peaks could be identified as shown in Figure 6.

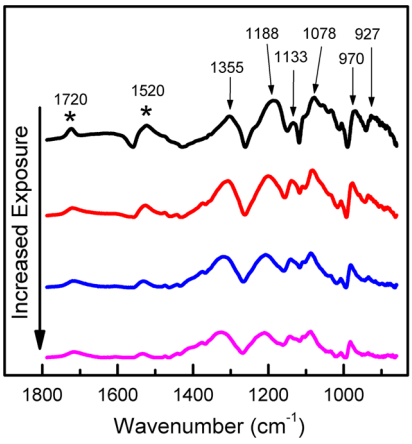

Figure 6. Enlarged region between 850 and 1800 cm^{-1} of the FTIR spectra with the baseline removed. Several modes of PEDOT:PSS have been labeled in the unexposed spectrum. Two modes significant to this study are highlighted by asterisks: a C═C mode at ∼1520 cm^{-1} and a mode associated with polymer doping at 1720 cm^{-1}. The unexposed film and films irradiated with 24.9, 48.3, and 71.6 J/cm^2 are shown with black, red, blue, and magenta lines, respectively.

A mode of particular interest to polymer chain length is that at ∼1520 cm^{-1}. The strength of this mode has been identified as an indicator of conjugation length of the PEDOT chain.[26] From the spectral results displayed in Figure 6, the C═C peak at 1520 cm^{-1} is observed to decrease with increasing exposure, corresponding to a reduction in material conductivity, which further supports the conformational changes in Raman spectra that correlated to the occurance of a scission event. Another feature of interest occurs at ∼1720 cm^{-1}. Although this mode does not explicitly identify with a specific molecular vibration, it has been reported elsewhere to correspond to the level of doping in PEDOT films.[27] In Figure 6, the continually decreasing strength of this mode with UV exposure is further evidence of a decline in doping and conductivity of the PEDOT:PSS films.

Additional distinct modes corresponding to PEDOT vibrations have been identified and are shown in Figure 7. It should be noted that these modes are all identified in the PEDOT structure and have not changed significantly in terms of strength. However, these modes were observed to undergo a shift to larger wavenumbers with UV exposure (Supporting Information, Figure S1). Figure 7 depicts this effect of UV irradiation as a shift away from the unexposed values, which are labeled on the *x*-axis. A theoretical treatment explaining this observed blue shift resulting from reduced conductivity is not available in the open literature. However, through observations generated in this study, it stands to reason that the blue shifts observed across many modes of the PEDOT chain arise due to reduced polymer chain lengths and subsequent changes in the energy of the molecular bonds.

Atomic force microscopy was performed to investigate physical morphological changes to the film. Dry PEDOT:PSS films have been found to maintain phase separation between the PEDOT and PSS regions inherent to an aqueous solution.

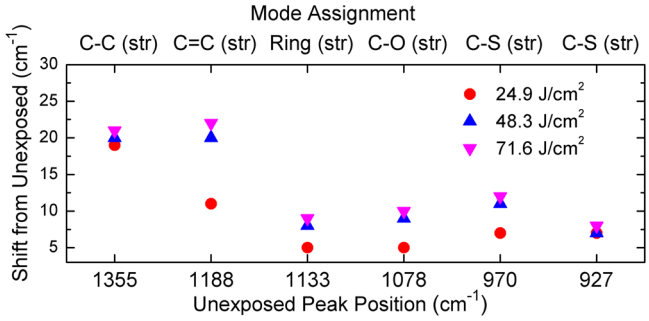

Figure 7. Assignment of FTIR peaks to PEDOT:PSS vibrational modes and observed blue-shifts of modes with increased UV exposure. The bottom horizontal axis indicates the peak position in the unexposed sample and the top horizontal axis identifies the associated vibrational mode.[21,24,25] Mode shifts for the film irradiated with 24.9, 48.3, and 71.6 J/cm^2 are shown in red, blue, and magenta, respectively.

This results in distinct regions between the conductive PEDOT areas surrounded by the insulating PSS shell.[28] When imaged by AFM, the film exhibits distinct elevated features that are associated with PEDOT surrounded by a subsided PSS background.[29] With such a structure, a higher surface roughness with distinct phase definition between PEDOT and PSS regions generally correlates to higher conductivity along the film itself. This is a result of preferential charge transfer through variable range hopping along continuous PEDOT chains as opposed to nearest neighbor hopping across insulating PSS boundaries. Figure 8 shows both the height and phase AFM images obtained from unexposed samples and those exposed to 71.6 J/cm^2 of UV radiation.

The unexposed films have a surface roughness measured to be R_a = 8.622 nm across a 400 μm^2 region, whereas the maximally exposed films have a roughness measured to be R_a = 2.398 nm. When examining the phase image of the unexposed sample, there is an even clearer distinction between various regions on the PEDOT:PSS surface; however, the exposed sample does not display this clear separation on the film surface. The reduced surface roughness and unclear phase distinction in the exposed sample is indicative of a significant change in the surface morphology. This change with UV exposure highlights a reduction in the size of the conductive PEDOT grains that are distinct and identifiable in the unexposed sample but are no longer obvious after UV irradiation. Although the Raman and FTIR spectra highlight a scission process that systematically truncates the PEDOT chain lengths and reduces material conductivity, the AFM images indicate reduced phase distinction between PEDOT and PSS regions on the surface of the thin film. This reduced phase distinction is likely a consequence of lower molecular weight PEDOT chains, allowing for permeation or reaction of PSS into PEDOT-rich regions.

Using spectroscopic ellipsometry (SE) characterization and subsequent thin film modeling, optical dispersion formulae for the PEDOT:PSS films were fitted by minimizing the difference between model simulations and experimental results. Because PEDOT:PSS is known to exhibit uniaxial anisotropy when spin-cast, dispersion curves were obtained for the film in the directions normal and parallel to the substrate between 0.6 and 5 eV.[30] The optical dispersion model used was a linear combination of a Drude and Lorentzian oscillator, which has previously been applied to PEDOT:PSS films with a high degree of accuracy.[31] As part of the optical modeling, the

DOI: 10.1021/am507981d
ACS Appl. Mater. Interfaces 2015, 7, 3940−3948

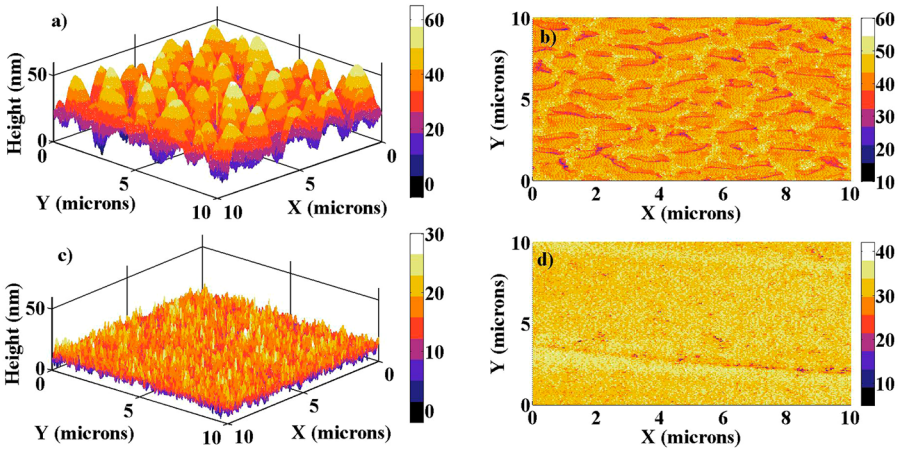

Figure 8. (a) AFM surface roughness of the unexposed PEDOT:PSS film on a glass substrate. (b) AFM phase, in units of degrees, of the unexposed PEDOT:PSS film displaying clear phase distinction between the PEDOT and PSS regions on the surface. (c) AFM surface roughness of the fully UV exposed PEDOT:PSS film. (d) AFM phase, in units of degrees, of the fully exposed PEDOT:PSS film displaying no clear phase distinction between the PEDOT and PSS regions.

thicknesses of the thin films were also extracted and compared to the thicknesses determined separately by AFM. Table 4 compares the optically determined thickness to that determined by AFM and can be seen to correlate within 5% for all cases.

Table 4. Film Thicknesses of PEDOT:PSS Films on a Silicon Substrate As Determined by AFM and SE

UV exposure (J/cm^2)	AFM film thickness (nm)	SE film thickness (nm)
0	204.1	211.4
24.9	171.6	170.2
48.3	155.5	155.8
71.6	147.1	151.8

In all samples, the spectroscopic model developed was found to fit very closely to the experimental results in the fitted energy regime (between 0.6 and 5 eV), and the error was on the order of a few percent. From the materials model, the complex index for both material orientations (ordinary and extraordinary, which are parallel and normal to the substrate, respectively) can be extracted.

Figure 9a and b show the real and imaginary components ($n^{=}$ and $k^{=}$, respectively) of the refractive index for the PEDOT:PSS film parallel to the substrate, and Figure 9c and d plot the real and imaginary components ($n^{\perp}$ and $k^{\perp}$, respectively) of the refractive index for the PEDOT:PSS films orthogonal to the substrate.

As observed in Figure 9 when comparing the differences between the ordinary and extraordinary indices of the pristine, unexposed PEDOT:PSS film, not only is there a lower value in the real refractive indices ($n^{=}$ relative to $n^{\perp}$), but also an accompanying higher imaginary component ($k^{=}$ relative to $k^{\perp}$). This observed anisotropy of the PEDOT:PSS film is similar to other reported accounts and is due to the spin-cast deposition resulting in PEDOT chains having their backbone primarily oriented parallel to the substrate.[30] This is in agreement with physical morphological studies indicating a lamellar structure of PEDOT:PSS from spin-casting.[28] From Figure 9, it can be seen that with increased UV exposure, both $n^{=}$ and $n^{\perp}$ increase at a given wavelength. This is attributed to densification of the PEDOT:PSS film brought about by the scission of polymer chain bonds. As the PEDOT chains become shorter, coupling

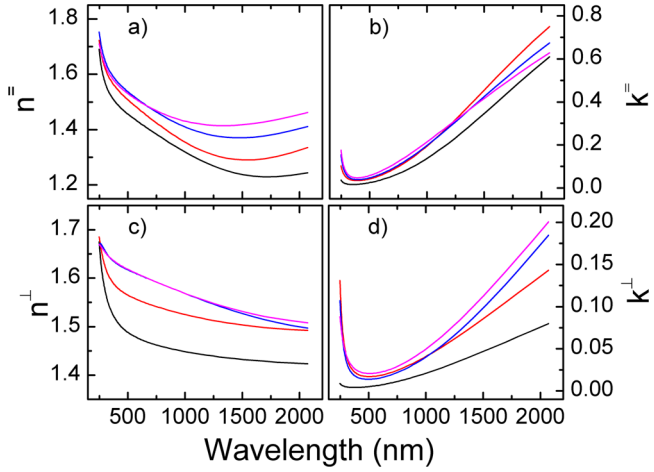

Figure 9. Dispersion relations for both the ordinary and extraordinary indices of a spin-cast PEDOT:PSS film and subsequent changes with UV exposure. Shown are the (a) real and (b) imaginary components of the refractive index ordinary to the substrate. Also shown are the (c) real and (d) imaginary components of the refractive index extraordinary to the substrate. In each dispersion relation, black, red, blue, and magenta curves correlate to the unexposed film and films irradiated with 24.9, 48.3, and 71.6 J/cm^2 of UV exposure, respectively.

between adjacent monomers is broken, allowing for permeation of other radicals or species into previously unoccupied vacancies in the film, which in turn results in densification of the film. The images from AFM that displayed a loss of phase distinction between the PEDOT and PSS regions (Figure 8b vs d) supplement the conjecture of chain scission along with film densification. This film densification results in an increase in the imaginary component of the refractive index in both directions ($k^{=}$ and $k^{\perp}$). Although there is a modest discrepancy in the progressive increase of $k^{=}$ in the near-IR wavelength regime of the film having undergone 71.6 J/cm^2 of UV exposure, this could result from a shift of the peak IR absorption outside the modeled region. Finally, it should be noted that the optical densification of the thin film as characterized by SE agrees with the reduction in film thickness that is observed with UV exposure. However, from the characterization methods utilized, it is impossible to determine whether this reduction is due

DOI: 10.1021/am507981d
ACS Appl. Mater. Interfaces 2015, 7, 3940−3948

solely to densification of the film, or whether there is an additional etching process occurring, as reported elsewhere.[17]

On the basis of the initial direct electrical measurements, it was found that UV exposure provides a notable increase in PEDOT:PSS thin film resistivity. The change in material resistivity is anisotropic in nature as a consequence of the initial anisotropic film morphology inherent to spin-cast deposition. Whereas the increase in resistivity in the ordinary index has been shown to increase over 4 orders of magnitude, that in the extraordinary direction only increases between 1 and 2 orders of magnitude.

The previous Raman and FTIR studies indicated a loss of vibrational signatures corresponding to a reduction in polymer chain length and a shift in PEDOT morphology from quinoid to benzoid. Combined with the reduced phase segregation between PEDOT and PSS regions highlighted from AFM analysis, the root effect of UV exposure is concluded to be a scission process along the conductive PEDOT chain. This conjecture additionally explains the difference in effects of UV radiation on the ordinary and extraordinary indices in the thin film. As the initial PEDOT:PSS creates a lamellar structure of conductive PEDOT grains separated by thin insulating PSS regions, electrical conduction is preferential in the direction parallel to the substrate, where PSS barriers are not as frequently encountered by charge carriers. Upon UV exposure, the scission event disrupts the inherent conductive pathways along the PEDOT chain. Then, rather than relatively long PEDOT chains conducive to carrier transport in the direction normal to the substrate, the film morphology consists of a number of thin PEDOT layers separated by a corresponding number of insulating PSS barriers. Upon UV exposure, the in-plane PEDOT chain length is still reduced resulting in a significant increase in the resistivity parallel to the substrate; however, it has less of an impact on carrier transport in the direction orthogonal to the substrate.

Because of the polymer scission process, the phase segregation between the PEDOT and PSS regions is disrupted, allowing for subsequent permeation of radical species and oxidation of the PEDOT:PSS film. This is evident in the refractive index dispersion curves, which display an increase in the complex refractive index due to film densification from the loss of phase segregation.

To demonstrate the utility of this etch-free patterning technique for applications in device fabrication, an example of devices that can benefit from this effect will be elucidated. OLEDs were fabricated using MEH:PPV as an active layer with PEDOT:PSS used as the hole transport layer. Despite UV irradiation, the PEDOT:PSS film still exhibits a high level of transparency across the visible regime (Supporting Information, Figure S1), preserving its suitability for OLED implementation. Two variations of these ITO/PEDOT:PSS/MEH:PPV/Al OLED devices were characterized: one with pristine PEDOT:PSS and a second with the PEDOT:PSS layer subjected to a dose of 71.6 J/cm^2 of UV exposure. The current−voltage characteristics are shown in the top graph of Figure 10. In the fully exposed diode, the current flow through decreases by approximately 1 to 2 orders of magnitude depending on the precise bias, correlating to an increase in the PEDOT:PSS film resistance. This subsequently leads to a corresponding reduction in light emission output. The optical output power relative to applied bias is shown in the bottom graph of Figure 10, which demonstrates that when the OLED is biased appropriately the device fabricated with unexposed

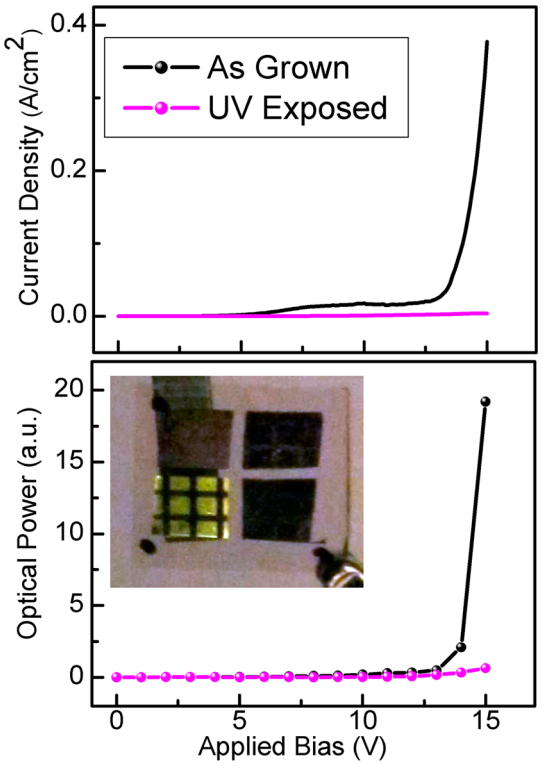

Figure 10. (top) $I-V$ of OLEDs fabricated using unexposed PEDOT:PSS (black line) or PEDOT:PSS having been subjected to 71.6 J/cm^2 of UV exposure (magenta line). (bottom) Corresponding optical output power from the OLED. (inset) Image of patterned LED grid using direct UV patterning.

PEDOT:PSS outputs power that is nearly an order of magnitude higher than that of its exposed counterpart. This is due to the voltage drop across the resistive PEDOT:PSS film such that the exposed diode does not reach turn-on until reaching a much higher bias.

A potential application of this process is to realize light emitting pixels with no material removal required. As such, a patterned OLED was fabricated exclusively through the application of UV radiation to the PEDOT:PSS layer. The inset of Figure 10 shows 4 arrays of OLED pixels. One of the arrays is biased to turn on, and light is emitted only from the regions with unexposed PEDOT:PSS. The exposure pattern is of 150 μm line widths with a separation of 500 μm of unexposed PEDOT:PSS. The key feature in this demonstration is that neither the ITO nor the Al contacts were patterned to obtain the patterned light emission nor was material physically removed from the layer stack. The entire device is composed of four completely intact layers, ITO, PEDOT:PSS, MEH:PPV, and Al, with no physical patterning, yet distinct pixels in the image can be easily identified.

CONCLUSION

A technique for patterning the conductivity of PEDOT:PSS using flood illumination from a UV source with a wavelength of 254 nm is demonstrated. Upon UV exposure of 71.6 J/cm^2, a PEDOT:PSS film exhibits an increase in lateral resistivity of more than 4 orders of magnitude. Because of the anisotropic morphological characteristics of these films, the increase in resistivity in the normal direction is limited to only 2 orders of magnitude. Raman characterization reveals a significant

DOI: 10.1021/am507981d
ACS Appl. Mater. Interfaces 2015, 7, 3940−3948

decrease of inter-ring stretching modes between PEDOT monomers, as well as a shift in film composition from the relatively conductive quinoid form of PEDOT to that of the less conductive benzoid formation. This reduction in material doping and conductivity is also corroborated using FTIR. Height and phase images of these films obtained from atomic force microscopy indicate a loss of phase segregation between the PEDOT grains and the PSS regions. Optical dispersion curves were extracted, and after UV irradiation, increases in the real and imaginary components of the refractive index were evident. This change is attributed to film densification. From the various analytical studies carried out, the increase in film resistivity can be attributed to polymer scission of the conductive PEDOT chains. In concert with this resistivity increase, the UV exposure resulted in a moderate height reduction (60−70% of initial thickness) along with an increase in the complex refractive index in the visible and near IR wavelengths. The sensitivity of PEDOT:PSS films to environmental UV light is well documented; however, it has rarely been utilized specifically for material processing and device fabrication. Although not studied in detail, the exposure to UV using these parameters did not result only in electrical conductivity patterning, but it also led to patterning in the film thickness. This can be explored to provide a facile route for realizing surface relief gratings by means of modulating the height of PEDOT:PSS with a predefined optical mask. Of particular interest to the optical and polymer optics community is the change in the refractive index with exposure as documented in this work. Additionally, this work has provided an optical dispersion model that fits well to the experimental data across visible and near-IR wavelengths. Accurate refractive index relation along with certain control over film characteristics is an enabling tool for optoelectronic device design. One application for this technology has been demonstrated by selectively patterning an OLED without material etching or resist development. Although the focus of this investigation and subsequent OLED demonstration was on tailoring the electrical conductivity of PEDOT:PSS films with UV exposure, the SE results highlight an additional area of interest whereby the film refractive indices can be optically patterned for use in a variety of novel optoelectronic applications. This approach has the potential to transform the manner by which organic optoelectronics are manufactured in large area devices.

■ ASSOCIATED CONTENT

Supporting Information

Measured values of FTIR modes with respect to UV irradiation and the effects of irradiation on the UV−vis absorption of the thin films. This material is available free of charge via the Internet at http://pubs.acs.org.

■ AUTHOR INFORMATION

Corresponding Author

*E-mail: a.helmy@utoronto.ca.

Notes

The authors declare no competing financial interest.

■ REFERENCES

(1) Forrest, S. R. The Path to Ubiquitous and Low-Cost Organic Electronic Appliances on Plastic. *Nature* **2004**, *428*, 911−918.
(2) Ouyang, J.; Xu, Q.; Chu, C.-W.; Yang, Y.; Li, G.; Shinar, J. On the Mechanism of Conductivity Enhancement in Poly(3,4-ethylenedioxythiophene):Poly(styrene sulfonate) Film Through Solvent Treatment. *Polymer* **2004**, *45*, 8443−8450.
(3) Groenendaal, L.; Jonas, F.; Freitag, D.; Pielartzik, H.; Reynolds, J. R. Poly(3,4-ethylenedioxithiophene) and Its Derivatives: Past, Present, and Future. *Adv. Mater.* **2000**, *12*, 481−494.
(4) Nardes, A. M.; Kemerink, M.; Janssen, R. A. J. Anisotropic Hopping Conduction in Spin-Coated PEDOT:PSS Thin Films. *Phys. Rev. B: Condens. Matter Mater. Phys.* **2007**, *76*, 085208.
(5) Granqvist, C. G.; Hultåker, A. Transparent and Conducting ITO Films: New Developments and Applications. *Thin Solid Films* **2002**, *411*, 1−5.
(6) Taylor, P. G.; Lee, J.-K.; Zakhidov, A. A.; Chatzichristidi, M.; Fong, H. H.; DeFranco, J. A.; Malliaras, G. G.; Ober, C. K. Orthogonal Patterning of PEDOT:PSS for Organic Electronics using Hydrofluoroether Solvents. *Adv. Mater.* **2009**, *21*, 2314−2317.
(7) Takakuwa, A.; Ikawa, M.; Fujita, M.; Yase, K. Micropatterning of Electrodes by Microcontact Printing Method and Application to Thin Film Transistor Devices. *Jpn. J. Appl. Phys., Part 1* **2007**, *46*, 5960−5963.
(8) Charlot, B.; Sassine, G.; Garraud, A.; Sorli, B.; Giani, A.; Combette, P. Micropatterning PEDOT:PSS Layers. *Microsyst. Technol.* **2013**, *19*, 895−903.
(9) Menard, E.; Meitl, M. A.; Sun, Y.; Park, J.-U.; Shir, D. J.-L.; Nam, Y.-S.; Jeon, S.; Rogers, J. A. Micro- and Nanopatterning Techniques for Organic Electronic and Optoelectronic Systems. *Chem. Rev.* **2007**, *107*, 1117−1160.
(10) Wong, T. K. S.; Gao, S.; Hu, X.; Liu, H.; Chan, Y. C.; Lam, Y. L. Patterning of Poly(3-alkylthiphene) Thin Films by Direct-Write Ultraviolet Laser Lithography. *Mater. Sci. Eng., B* **1998**, *55*, 71−78.
(11) Kim, W.; Kafafi, Z. Method of Patterning Electrically Conductive Polymers. U.S. Patent 6,649,327 B2, November 18, 2003.
(12) Lin, Y.-J.; Yang, F.-Y.; Huang, C.-Y.; Chou, W.-Y.; Chang, J.; Lien, T.-C. Increasing the Work Function of Poly(3,4-ethylenedioxythiophene) Doped with Poly(4-styrenesulfonate) by Ultraviolet Radiation. *Appl. Phys. Lett.* **2007**, *91*, 092127.
(13) Moujoud, A.; Oh, S. H.; Shin, H. S.; Kim, H. J. On the Mechanism of Conductivity Enhancement and Work Function Control in PEDOT:PSS Film Through UV-Light Treatment. *Phys. Status Solidi A* **2010**, *207*, 1704−1707.
(14) Nagata, T.; Oh, S.; Chikyow, T.; Wakayama, Y. Effect of UV-Ozone Treatment on Electrical Properties of PEDOT:PSS Film. *Org. Electron.* **2011**, *12*, 279−284.
(15) Benor, A.; Takizawa, S.; Chen, P.; Pérez-Bolívar, C.; Anzenbacher, P., Jr. Dramatic Efficiency Improvement in Phosphorescent Organic Light-Emitting Diodes with Ultraviolet-Ozone Treated Poly(3,4-ethylenedioxythiophene):Poly(styrenesulfonate). *Appl. Phys. Lett.* **2009**, *94*, 193301.
(16) Lee, H. K.; Kim, J.-K.; Park, O. O. Effects of UV Light-Irradiated Buffer Layer on the Performance of Polymer Solar Cells. *Org. Electron.* **2009**, *10*, 1641−1644.
(17) Benor, A.; Takizawa, S.; Pérez-Bolívar, C.; Anzenbacher, P., Jr. Efficiency Improvement of Fluorescent OLEDs by Tuning the Working Function of PEDOT:PSS Using UV-Ozone Exposure. *Org. Electron.* **2010**, *11*, 938−945.
(18) Schrote, K.; Frey, M. W. Effect of Irradiation on Poly(3,4-ethylenedioxythiophene):Poly(styrenesulfonate) Nanofiber Conductivity. *Polymer* **2013**, *54*, 737−742.
(19) Eleschner, A.; Kirchmeyer, W.; Lövenich, W.; Merker, U.; Reuter, K. *PEDOT: Principles and Applications of Intrinsically Conductive Polymer*; CRC Press: Boca Raton, FL, 2011; pp 126−128.
(20) Schaarschmidt, A.; Farah, A. A.; Aby, A.; Helmy, A. S. Influence of Nonadiabatic Annealing on the Morphology and Molecular Structure of PEDOT:PSS Films. *J. Phys. Chem. B* **2009**, *113*, 9352−9355.
(21) Garreau, S.; Louarn, G.; Buisson, J. P.; Froyer, G.; Lefrant, S. In Situ Spectroelectrochemical Raman Studies of Poly(3,4-ethylenedioxythiophene) (PEDT). *Macromolecules* **1999**, *32*, 6807−6812.

DOI: 10.1021/am507981d
ACS Appl. Mater. Interfaces 2015, 7, 3940−3948

(22) Lapkowski, M.; Pron, A. Electrochemical Oxidation of Poly(3,4-ethylenedioxythiphene) − "In Situ" Conductivity and Spectroscopic Investigations. *Synth. Met.* **2000**, *110*, 79−83.
(23) Kvarnström, C.; Neugebauer, H.; Ivaska, A.; Sariciftci, N. S. Vibrational Signatures of Electrochemical *p*- and *n*-Doping of Poly(3,4-ethylenedioxythiophene) Films: An In Situ Attenuated Total Reflection Fourier Transform Infrared (ATR-FTIR) Study. *J. Mol. Struct.* **2000**, *521*, 271−277.
(24) Kvarnström, C.; Neugebauer, H.; Blomquist, S.; Ahonen, H. J.; Kankare, J.; Ivaska, A. In Situ Spectroelectrochemical Characterization of Poly(3,4-ethylenedioxythiophene). *Electrochim. Acta* **1999**, *44*, 2739−2750.
(25) Tran-Van, F.; Garreau, S.; Louarn, G.; Froyer, G.; Chevrot, C. Fully Undoped and Soluble Oligo(3,4,-ethylenedioxythiophene)s: Spectroscopic Study and Electrochemical Characterization. *J. Mater. Chem.* **2001**, *11*, 1378−1382.
(26) Im, S. G.; Gleason, K. K. Systematic Control of the Electrical Conductivity of Poly(3,4-ethylenedioxythiophene) via Oxidative Chemical Vapor Deposition. *Macromolecules* **2007**, *40*, 6552−6556.
(27) Selvaganesh, S. V.; Mathiyarasu, J.; Phani, K. L. N.; Yegnaraman, V. Chemical Synthesis of PEDOT-Au Nanocomposite. *Nanoscale Res. Lett.* **2007**, *2*, 546−549.
(28) Nardes, A. M.; Kemerink, M.; Janssen, R. A. J.; Bastiaansen, J. A. M.; Kiggen, N. M. M.; Langeveld, B. M. W.; van Breeman, A. J. J. M.; de Kok, M. M. Microscopic Understanding of the Anisotropic Conductivity of PEDOT:PSS Thin Films. *Adv. Mater.* **2007**, *19*, 1196−1200.
(29) Farah, A. A.; Rutledge, S. A.; Schaarschmidt, A.; Lai, R.; Freedman, J. P.; Helmy, A. S. Conductivity Enhancement of Poly(3,4-ethylenedioxythiophene)-Poly(styrenesulfonate) Films Post-Spin-casting. *J. Appl. Phys.* **2012**, *112*, 113709.
(30) Pettersson, L. A. A.; Ghosh, S.; Inganäs, O. Optical Anisotropy in Thin Films of Poly(3,4-ethylenedioxythiophene)-Poly(4-styrenesulfonate). *Org. Electron.* **2002**, *3*, 143−148.
(31) Iso, T.; Hayashi, T.; Ueno, K.; Shirai, H. Atmospheric-Pressure Argon Plasma Etching of Spin-Coated 3,4-polyethylenedioxythiophene:polystyrenesulfonic Acid (PEDOT:PSS) Films for Cupper Phyalocyanine (CuPc)/C_{60} Heterojunction Thin-Film Solar Cells. *Thin Solid Films* **2011**, *519*, 6834−6839.

DOI: 10.1021/am507981d
ACS Appl. Mater. Interfaces 2015, 7, 3940−3948